Astron. Astrophys. 337, 125–140 (1998)

ASTRONOMY AND ASTROPHYSICS

The overlapping open clusters NGC 1750 and NGC 1758

III. Cluster-field segregation and clusters physical parameters

D. Galadí-Enríquez[1], **C. Jordi**[1], **and E. Trullols**[1,2]

[1] Dept. d'Astronomia i Meteorologia, Univ. de Barcelona, Avda. Diagonal 647, E-08028 Barcelona, Spain
[2] Dept. de Matemàtica Aplicada i Telemàtica, Univ. Politècnica de Catalunya, Avda. Víctor Balaguer s/n, E-08800 Vilanova i la Geltrú, Spain

Received 2 March 1998 / Accepted 22 June 1998

Abstract. Cluster-field segregation and determination of physical parameters of the open clusters NGC 1750 and NGC 1758 were performed from CCD and photographic photometric and astrometric surveys previously published by the authors. Membership probabilities were computed to a brightness limit of $R = 15$ mag through a non-standard method in a fully non-parametric approach, using proper motions, positions and photometry.

This study allowed several parameters for NGC 1750 and NGC 1758 to be determined, including position, size, density profile, absorption, distance, age, luminosity function and mass. The common colour excess of both clusters is $E(B-V) = 0.34$ mag. NGC 1750 is slightly younger ($\log t = 8.3$), closer ($V - M_v = 9.0$ mag) and less concentrated than NGC 1758 ($\log t = 8.60$ and $V - M_v = 9.4$ mag). We also conclude that NGC 1746 is an erroneous assignation (not corresponding to any real open cluster), and that NGC 1750 and NGC 1758 are overlapping clusters, but they do not constitute a gravitationally bounded system.

Key words: open clusters and associations: individual: NGC 1746 – open clusters and associations: individual: NGC 1750 – open clusters and associations: individual: NGC 1758 – stars: luminosity function, mass function – methods: statistical

1. Introduction

Very close to the galactic anticenter, in the direction of the Taurus dark cloud complex, Dreyer (1888), in his *New General Catalogue of Nebulae and Clusters of Stars*, identifies three partially overlapping clusters in a radius of $\sim 20'$: NGC 1746, NGC 1750 and NGC 1758. The IAU official designations are C 0500+237, C 0500+235 and C 0501+237, respectively. The existence and nature of these clusters have been a matter of discussion over recent decades. The main studies of this zone include the photographic photometric survey by Cuffey (1937) and the Vilnius photoelectric work by Straižys et al. (1992a, referred to as SČM from now on).

Send offprint requests to: D. Galadí-Enríquez
Correspondence to: dgaladi@pchpc5.am.ub.es

This paper is the last in a series devoted to a comprehensive astrometric and photometric analysis of this zone, with the aim of clarifying the existence of these objects and determining their main physical parameters. The first article (Galadí-Enríquez et al. 1998a, from now on referred to as Paper I) dealt mainly with a *UBVRI*-CCD photometric survey of 3224 stars in a radius of about $15'$ around the center of NGC 1750. Paper I also contains a brief introduction to the observational history of the area, and we refer to it for the search of literature about the clusters. The second article (Galadí-Enríquez et al. 1998b, hereafter referred to as Paper II) provided a catalogue with 51846 stars, 39762 of them with photographic photometry, and 45036 of them with proper motions, in an area of $2.3^\circ \times 2.3^\circ$ around the cluster centers.

A raw analysis performed on the data from Paper I and Paper II, assigning members to each cluster from a strictly spatial point of view, indicated the true presence of two open clusters in the area. The main sequences of the objects are clearly defined, but they overlap to a large extent and cannot be easily separated using only photometric data. Astrometric information confirmed the existence of two separate objects identifiable with NGC 1750 and NGC 1758. These raw analyses did not show any astrometric nor photometric evidence for NGC 1746.

In the present paper we perform a detailed analysis of the observational data from Paper I and Paper II. Our goals are the cluster-field segregation, and the determination of the main physical parameters of the clusters. As the clusters are sparse and poor, the field star distribution dominates the proper motion vector point diagram, hindering the separation of the cluster populations. To improve the efficiency of membership determination, we combined proper motions, spatial coordinates and photometry. The field and cluster frequency functions in all three observational planes were determined in a fully non-parametric approach, by using kernel functions, leading to individual membership probabilities. Further analysis of the stars selected as members, allowed us to determine positions, density profiles, absorption, distances, sizes, ages, luminosity functions and mass estimates for the open clusters NGC 1750 and NGC 1758.

This paper is organized into 6 main sections. In Sect. 2 we describe the general mathematical foundations of the member-

ship probability calculations, and a basic discussion on the non-parametric determination of frequency functions by means of kernel functions. Sect. 3 is devoted to the application of this method to our observational data, and includes a brief discussion of the field and cluster frequency functions. The selection of the stars accepted as members of NGC 1750 and NGC 1758 is described in Sect. 4, leading to the determination of the physical parameters of the clusters in Sect. 5. The conclusions are summarized in Sect. 6.

2. Membership probabilities from empirical frequency functions

As mentioned in the previous section, the clusters in the studied area are loose and poor. Their low contrast against the field population, and the need to separate from the field not one, but two spatially and photometrically overlapping clusters, makes the segregation problem critical. We decided to combine all available information, applying a non-parametric method for the determination of the probability density functions. In this section we describe the basic mathematical foundations of the process and we establish the definitions and notation used throughout this paper. We also outline the disadvantages of the classical parametric methods when applied to our case.

2.1. Membership probabilities: general formulation

Let us consider a two-dimensional space with coordinates (a, b), in which we have two superimposed samples with N_1 and N_2 individuals spread according to two different probability density functions (pdf), $\phi_1(a, b)$ and $\phi_2(a, b)$. The samples follow the frequency functions:

$$\Phi_i(a, b) = N_i \;\; \phi_i(a, b), \qquad i = 1, 2, \tag{1}$$

with:

$$\int_{-\infty}^{+\infty} \int_{-\infty}^{+\infty} \phi_i(a, b) \; \mathrm{d}a \; \mathrm{d}b = 1, \quad i = 1, 2. \tag{2}$$

According to Bayesian theory, for an individual found in the 2-D space at position (a, b), the probability of belonging to population i is:

$$P_i(a, b) = \frac{\Phi_i(a, b)}{\sum_{j=1}^{2} \Phi_j(a, b)}, \qquad i = 1, 2. \tag{3}$$

The usual approach to membership determination in open clusters solves the problem in the proper motion space, i.e., $(a, b) = (\mu_x, \mu_y)$, called the 'kinematic plane' in this study. The cluster segregation is reduced to the determination of the field and cluster frequency functions. Individual membership probabilities are assigned to each star according to Eq. 3, allowing to select the cluster members.

2.2. Frequency functions: parametric models

Most membership studies on open clusters apply a version of the classical Vasilevskis-Sanders method (Vasilevskis et al. 1958, Vasilevskis et al. 1965, Sanders 1971), in which cluster and field frequency functions in the kinematic plane are modelized as bivariate gaussian distributions. Usually, a circular normal distribution is assumed for the cluster population, while the field is considered to be well represented by an elliptic normal distribution. The model parameters are determined in an iterative process based on the maximum likelihood method (Hand 1981).

Many different implementations of this method have been in use over the last decades. Some of them involve slight simplifications (such as the removal of the covariance parameter through an axis rotation, Slovak 1977), and most of them are improved versions including additional features, such as taking into account the individual errors of the proper motions (Stetson 1980, Zhao & He 1990), performing a rigorous pruning of outliers before the model is fitted (Cabrera-Caño & Alfaro 1985) or considering the spatial distribution of stars.

This last point deserves more attention. Open clusters are in almost all cases identified and catalogued thanks to their spatial concentration: they have a surface density of stars that makes them stand out in the sky among the field. The inclusion of this spatial information enlarges the statistical distance between the field and cluster populations. Usually, this has been done by assuming a parametric model, following gaussian, King's or exponential functions for the cluster density profiles and a flat distribution for the field (see for instance, Kozhurina-Platais et al. 1995, Zhao & Shao 1994).

2.3. Drawbacks of the parametric approach

Membership determinations based on parametric pdf fits in the kinematic plane are widespread, and, in general, they are considered to yield the most reliable cluster-field segregations. But it is necessary to keep in mind the implicit assumptions and intrinsic limitations of this method, as pointed out by Cabrera-Caño & Alfaro (1990). Reference should be made to these authors for a more detailed discussion and for the relevant papers concerning this question. Here, we highlight the main drawbacks of the parametric approach when applied to our observational data.

A circular bivariate function is a good representation of the cluster pdf, if the intrinsic velocity dispersion of the cluster is not resolved and there are no systematic differences of accuracy between the two proper motion axes in the observational material. The choice of an elliptic bivariate gaussian function for the field distribution is known to be unrealistic. The proper motion distribution of field stars has an intricate structure dominated by the combination of solar motion and galactic differential rotation. Depending on the direction of observation and the proper motion accuracy, several asymmetries arise, the most evident of which is the tail in the direction of the solar antiapex (Paper II). Furthermore, real field distribution wings are stronger than those predicted by a gaussian model (Marschall & Van Altena 1987).

This said, when dealing with a rich cluster whose population dominates the observed sample, the model adopted for the field is not crucial when deriving the cluster parameters. When the field population can be compared in size to the cluster sample, or when (as in our case) the field population is dominant, the residuals of an inaccurate field model can be of the same order or bigger than the cluster signal, and the membership calculations might be severely affected.

These effects are evident, for example, in the Pleiades survey by Schilbach et al. (1995). Those authors faced a situation similar to ours to some extent: their direction of observation was in Taurus, and the field population was numerically dominant. They needed to apply a field pdf model formed from two independent elliptical gaussian functions. Although the fit was not perfect this model was adequate for their purposes, because the Pleiades motion is very well separated from the mean field motion. In her study of galactic structure, Soubiran (1992) modelized the field population in the direction of the North Galactic Pole by means of the sum of three gaussian distributions.

In our case, as seen in the preliminary analysis performed in Paper II, the clusters mean proper motions are close to the maximum of the field distribution (the distances to this maximum are smaller than 3 mas yr^{-1}), and the clusters are not as rich as Pleiades: an accurate model of the field distribution is crucial for us.

We performed different tests with a classical parametric Vasilevskis-Sanders-based method, incorporating several modifications. The most obvious change was the inclusion of not one, but two circular bivariate gaussians to model the two clusters. In order to improve the contrast of the clusters against the field population, we limited the sample to the brighter stars, and stars with a proper motion error greater than 2.5 mas yr^{-1} were omitted. Modeling the field pdf with just one elliptical gaussian proved to be very unsatisfactory. When using such a model, one of the two circular gaussians originally intended to represent the clusters was moved by the procedure into the field population after a few iterations, indicating that only one elliptic gaussian is not enough to represent the field.

A second elliptical gaussian was added to the model. At this point, the procedure involved the fitting of four gaussian distributions. The convergence was unstable, with cluster (circular) distributions migrating towards the field and vice-versa. The results were highly dependent on the initial values of the parameters and on the sample cutoffs in brightness and in proper motion error. Attempts were carried out to fit the two field gaussians in the plate zones where we did not expect to find cluster members and, with these distributions already fixed, we determined the two circular cluster distributions. The poor results obtained indicated that we should adopt a wholly different approach: the empirical determination of the pdf's using kernel functions.

2.4. Frequency functions: non-parametric method

A non-parametric method for open cluster segregation was proposed by Cabrera-Caño & Alfaro (1990). The key is to perform an empirical determination of the pdf's, without relying on any previous assumption about their profiles. Being a general method, it can be applied in the kinematic as in other observational planes. In this section we describe our implementation of this approach.

For a sample of N individuals distributed in a two-dimensional space with coordinates (a, b), it is possible to tabulate the frequency function $\Phi(a, b)$ by evaluating the observed local density at each node of a grid of $n_a \times n_b$ points extended over the region of interest in the space. If this grid is dense enough, the empirical frequency function $\{\Psi(a_i, b_j); i = 1, \cdots, n_a; j = 1, \cdots, n_b\}$ will be equivalent, for all practical purposes, to the true $\Phi(a, b)$.

The easiest way to estimate the local density around a point (a_i, b_j) is by centering a transparent circular window of radius r on it, counting all the individuals seen through the window and dividing the resulting number by the circle area πr^2. The kernel estimator technique (Hand 1982) is simply a generalization of this idea. Instead of a transparent window with sharp border, this method uses a window with arbitrary shape, and with a transparency which decreases evenly from the center outwards, following a definite profile described by the so-called *kernel function*, $K(a, b)$. The value of the kernel function acts as a weight which can be applied to the individuals seen through the window, when counting them. The division by the effective area of the window is automatically incorporated into the process if the kernel function is normalized:

$$\int_{-\infty}^{+\infty} \int_{-\infty}^{+\infty} K(a, b)\ \mathrm{d}a\ \mathrm{d}b = 1.$$

So, the sharp border circular window can be considered as a kernel function that, centered at point (a_i, b_j), is written:

$$K(a, b) = \begin{cases} \frac{1}{\pi r^2} & \text{if } [(a - a_i)^2 + (b - b_j)^2] < r^2 \\ 0 & \text{otherwise.} \end{cases}$$

Kernel functions can be arbitrary in shape, but for most applications radially symmetrical functions are preferred. In this study we used normal circular kernels of the form:

$$K(a, b) = \frac{1}{2\pi h^2} \exp\left[-\frac{1}{2}\ \frac{(a - a_i)^2 + (b - b_j)^2}{h^2}\right].$$

In these conditions, our empirical frequency function Ψ becomes, for each point $\{(a_i, b_j); i = 1, \cdots, n_a; j = 1, \cdots, n_b\}$ of the grid:

$$\Psi(a_i, b_j) = \sum_{k=1}^{N} K(a_k, b_k),$$

where (a_k, b_k) are the coordinates of the k-th individual of the observed sample.

The parameter h (gaussian dispersion) acts as the effective radius of the window, and is usually called the smoothing parameter. A large h value would blur out the details of the true

frequency function, while a small h would yield a noisy result, because a very low effective number of individuals would be contained in the kernel window. The empirical $\Psi(a_i, b_j)$ and the true $\Phi(a, b)$ frequency functions would coincide in the limit $h \to 0$, but this value could not be used unless the sample was formed by an infinite number of individuals $N \to \infty$. There are several criteria for selecting the optimum h for a given sample. As Chen et al. (1997), we have followed Silverman's (1986) rule, that, for normal circular kernels, yields:

$$h = \left(\frac{4}{d+2} \right)^{1/(d+4)} \sigma \; N^{-1/(d+4)},$$

where d is the dimension of the space (in our case, $d = 2$), and σ is the average marginal variance, defined as $\sigma^2 = \sum \sigma_i^2 \; /d$, being $\sigma_i (i = 1, \cdots, d)$ the standard deviation of the observed sample coordinates.

Transform the empirical frequency function $\Psi(a_i, b_j)$ into the empirical probability density function $\psi(a_i, a_j)$ can be carried out in a straightforward manner by normalizing to unit volume:

$$\psi(a_i, b_j) = \Psi(a_i, b_j) \left[\sum_{k=1,m=1}^{n_a, n_b} \Psi(a_k, b_m) \; \Delta a \; \Delta b \right]^{-1},$$

where Δa and Δb are the grid cell sizes.

3. Empirical frequency functions: application to our sample

The empirical method described in the previous section was applied to the astrometric and photometric catalogue from Paper II. Since the formulation is general, we did not restrict ourselves to the kinematic (μ_x, μ_y) plane. In order to increase the statistical distance of the populations, we treated the spatial (x, y) and photometric (*R,B–R*) planes similarly. In each observational plane, we considered the existence of *two* superimposed populations, one of which is the 'field' population, while the other is the 'non-field' or 'clusters' population, which comprises all possible clusters in the studied area. In this way, we do not introduce any assumption about the possible number of clusters present in the zone.

We applied the process independently to each plane, according to the two-dimensional formulation of Sect. 2. We could have opted for a general six-dimensional space, combining all the variables following the n-dimensional formulation of the kernel estimator theory (see for instance, Chen et al. 1997 and references therein). But, as Cabrera-Caño & Alfaro (1990), we preferred to deal with each observational space separately: keeping the planes apart allows a direct physical interpretation of the resulting frequency functions and membership probabilities in each observational space.

The procedure described in this section was tested for several subsamples, selected by applying different magnitude, proper motion and proper motion error cutoffs. The results are reported for a subsample which was limited in the following way:

- proper motion cutoff: $\sqrt{\mu_x^2 + \mu_y^2} \leq 6$ mas yr^{-1}
- proper motion error cutoff: $\sqrt{\sigma_{\mu x}^2 + \sigma_{\mu y}^2} \leq 2.5$ mas yr^{-1}
- magnitude cutoff: $R \leq 15$ mag

In addition, to avoid plate border effects and to limit the field contribution in the sample, the region studied was a circle centered on the cluster zone and with radius 45′. The resulting set of stars, from now on called 'the selected sample', contains 1221 stars. As shown by the preliminary analysis performed in Paper II, the selected proper motion cutoff contains the complete interval of values in which cluster members are to be found. Very few stars have errors bigger than the proper motion error cutoff in the magnitude interval selected. As for the brightness limit, it is well known that the field population grows exponentially with magnitude, while a large fraction of open cluster luminosity functions seem to be flat at the faint end, and this would seem to be the case here (Sect. 5.4). The continuous growth in observational errors and number of field stars with magnitude means the clusters are hidden by the field in the low brightness intervals. Our limit of $R = 15$ mag was found to be a good compromise solution between photometric depth and reliable segregation results.

3.1. Kinematic plane: proper motions

The kinematic plane proved to be the best for cluster-cluster segregation in our case, because their proper motion distributions appeared clearly separated from each other.

Applying a kernel density estimator, the resulting empirical frequency function $\Psi^{\rm k}_{\rm c+f}$ contains the sum of the two underlying populations: $\Psi^{\rm k}_{\rm c+f} = \Psi^{\rm k}_{\rm c} + \Psi^{\rm k}_{\rm f}$, where 'c' stands for 'clusters', 'f' for 'field' and 'k' labels the kinematic plane. To know $\Psi^{\rm k}_{\rm c}$, it is necessary to decompose $\Psi^{\rm k}_{\rm c+f}$ by estimating the field contribution. Chen et al. (1997) faced a similar problem in their four-dimensional space, and they assumed a parametric (gaussian) shape for the field frequency function. Chen et al. (1998) preferred to subtract the field contribution estimating this from predictions given by a Galaxy model. In our case, the preliminary analysis of the data (Paper II) showed that the zone surveyed covers plenty of space where cluster contributions are negligible. Taking advantage of this situation, and making the fundamental assumption that the field pdf in the kinematic plane does not significantly change over the zone studied, we proceeded as follows.

We set a circle centered on the clusters zone, with radius $\rho = 25'$, estimated as containing all the significant contribution from the cluster populations. The kernel density estimator was applied in the kinematic plane to these data, yielding the empirical frequency function $\Psi^{\rm k}_{\rm c+f}$, for a grid with cell size of 0.08 mas yr^{-1}, well below the proper motion errors.

We set a corona centered on the cluster zone, with inner and outer radii $\rho_o = 30'$ and $\rho_1 = 45'$, respectively. The cluster stellar densities are estimated to be negligible in this area. We applied the kernel density estimator to the data inside this corona. We additionally assumed that the spatial stellar density of the

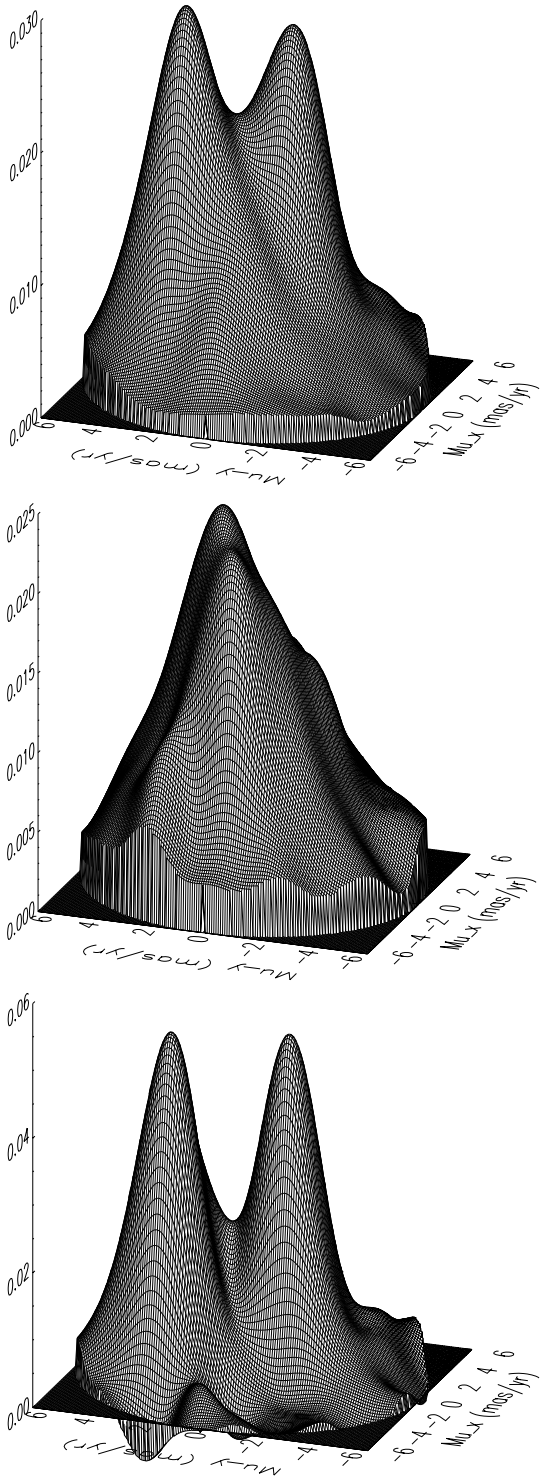

Fig. 1. Kinematic empirical pdf's. Top: mixed sample($\psi^{\rm k}_{\rm c+f}$) from the inner circle of radius $25'$. Center: field population ($\psi^{\rm k}_{\rm f}$) from the corona between $30'$ and $45'$. Bottom: non-field, or clusters population ($\psi^{\rm k}_{\rm c}$) from the inner circle of radius $25'$

field population was approximately uniform over the whole area surveyed and, so, the resulting field frequency function in the corona $\Psi^{\rm k}_{\rm f'}$ can be scaled to represent the field frequency function in the inner circle $\Psi^{\rm k}_{\rm f}$ by simply applying an area factor $\rho^2/(\rho_1^2-\rho_o^2)$.

After these operations, the cluster empirical frequency function in the kinematic plane can be determined as $\Psi^{\rm k}_{\rm c}=\Psi^{\rm k}_{\rm c+f}-\Psi^{\rm k}_{\rm f}$. These empirical frequency functions can be normalized to yield the empirical pdf's for the mixed population (circle), for the field (from the corona) and for the clusters (non-field) population: $\psi^{\rm k}_{\rm c+f}$, $\psi^{\rm k}_{\rm f}$, and $\psi^{\rm k}_{\rm c}$. Fig. 1 displays these three functions. The contribution of the clusters is evident in the mixed pdf $\psi^{\rm k}_{\rm c+f}$, and they are clearly outstanding in the non-field pdf $\psi^{\rm k}_{\rm c}$. If the empirical kinematic frequency functions are identified with the true frequency functions, the empirical tables can be used to measure the kinematic probability of not being a field star in a similar way to Eq. 3. If N_c is the number of cells along both axes, for each node of the grid $\{(\mu_{xi},\mu_{yj});i,j=1,\cdots,N_c\}$ the kinematic probability of a star placed on it being a member of the cluster population is:

$$P^{\rm k}_{\rm c}(\mu_{xi},\mu_{yj})=\frac{\Psi^{\rm k}_{\rm c+f}(\mu_{xi},\mu_{yj})-\Psi^{\rm k}_{\rm f}(\mu_{xi},\mu_{yj})}{\Psi^{\rm k}_{\rm c+f}(\mu_{xi},\mu_{yj})} \quad (4)$$

This array permits the empirical assignation of individual kinematic membership probabilities to the stars in the selected sample, according to the probability of their nearest node.

It is evident in Fig. 1 that the field pdf estimated in the outer corona is not a perfect representation of the true field pdf in the inner circle. This introduces undesired noise in the function $\psi^{\rm k}_{\rm c}$, as shown by the negative density values found in several zones. These negative values allowed us to estimate the typical noise level, γ, present in the result. To avoid meaningless probabilities in zones of low density, we restricted the probability calculations (Eq. 4) to the stars with $\psi^{\rm k}_{\rm c}\geq 3\gamma$.

It should be noticed that the heights and volumes of both cluster distributions are comparable, implying that they have similar numbers of member stars. Since the clusters are known to be very different in angular dimensions, this implies a noticeable difference in the surface density of stars. In fact, NGC 1758 was already known to be denser than NGC 1750 from the preliminary analysis of the data (Paper II). The maxima of $\psi^{\rm k}_{\rm c}$ are located at $(\mu_x,\mu_y)=(-1.5,2.5)$ mas yr^{-1}, and $(0.6,-1.2)$ mas yr^{-1}. The distance between both maxima is 4.2 mas yr^{-1}. From the conclusions of Paper I and Paper II, it is possible to identify the first cluster with NGC 1750, and the second one with NGC 1758. No kinematic indication of NGC 1746 was found. Applying the transformations to the equatorial system from Paper II, the absolute proper motions of the clusters in the ICRS reference system are $(\mu_\alpha\cos\delta,\mu_\delta)=(-3.0,-6.0)$ mas yr^{-1} for NGC 1750, and $(+0.7,-8.1)$ mas yr^{-1} for NGC 1758.

3.2. Spatial plane: x and y coordinates

The kernel density estimator method was applied to the selected sample in the spatial plane inside the circle centered on the cluster zone, with radius $\rho=25'$. We set a grid with nodes separated by 0.307 mm as in both x and y coordinates. This gives a cell size of $20''\times 20''$ that leads to an average stellar density of about

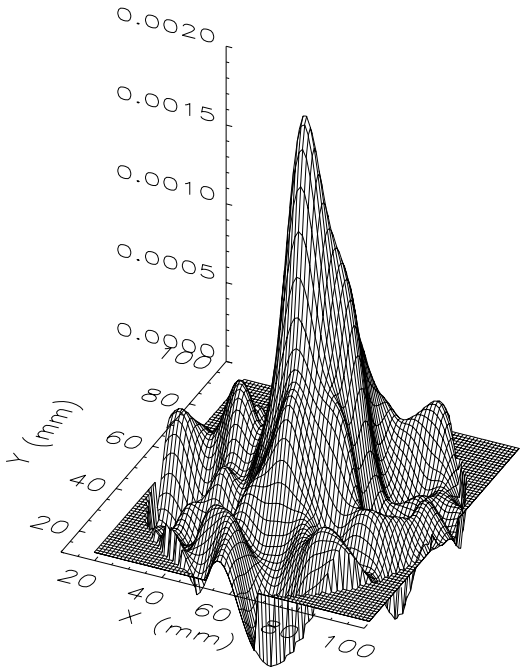

Fig. 2. Spatial empirical pdf $\psi_{\rm c}^{\rm s}$ over a circle with radius $45'$ around the cluster center, after subtraction of the field contribution. The field density was evaluated by fitting a tilted plane to the density distribution found inside a corona with inner and outer radii of $30'$ and $45'$. The strongest central concentration corresponds to the location of NGC 1758, while the asymmetric overdensity around this peak can be attributed to NGC 1750. The scale is $65.25''$ mm^{-1}

0.07 stars per cell. The resulting empirical frequency function $\Psi_{\rm c+f}^{\rm s}$ (where 's' stands for 'space') should be decomposed into field and non-field (clusters) contributions: $\Psi_{\rm c+f}^{\rm s} = \Psi_{\rm c}^{\rm s} + \Psi_{\rm f}^{\rm s}$.

In order to estimate the field spatial density distribution, we computed the spatial frequency function $\Psi_{\rm f'}^{\rm s}$ in a corona centered on the cluster zone, with inner and outer radii $\rho_o = 30'$ and $\rho_1 = 45'$, as we did in the kinematic plane. To extrapolate this frequency function to the inner circle, we fitted a tilted plane to the distribution found in the corona. The tilt was found to be very slight, and this validates the assumption made in the previous section concerning the uniformity of the spatial stellar density of the field. This tilted plane was assumed to represent the field spatial frequency function in the inner circle $\Psi_{\rm f}^{\rm s}$ and was subtracted from the mixed distribution.

The spatial pdf's $\psi_{\rm c+f}^{\rm s}$, $\psi_{\rm f}^{\rm s}$ and $\psi_{\rm c}^{\rm s}$ were obtained from the frequency functions by normalizing to unit volume. The resulting cluster pdf is shown in Fig. 2. Negative values and bumps provide evidence of the small-scale fluctuations of the field stellar density. The highest density coincides with the position of NGC 1758, while the asymmetric distribution around the maximum can be attributed to NGC 1750 population. As it is known, the two clusters are not well separated in space: thus while the spatial plane can provide probabilities of a star not being a field star, it is less efficient than the kinematic plane for distinguishing NGC 1750 and NGC 1758 contributions. For a star placed at the node $\{(x_i, y_j); i, j = 1, \cdots, N_c\}$ of the grid, the spatial probability of it not being a field star is computed as:

$$P_{\rm c}^{\rm s}(x_i, y_j) = \frac{\Psi_{\rm c+f}^{\rm s}(x_i, y_j) - \Psi_{\rm f}^{\rm s}(x_i, y_j)}{\Psi_{\rm c+f}^{\rm s}(x_i, y_j)}. \quad (5)$$

3.3. Photometric plane: photographic colour-magnitude diagram

Preliminary analysis (Paper I and Paper II) showed an outstanding main sequence in the colour-magnitude diagram, related to the clusters present in the zone. This photometric contrast can be used to assign photometric membership probabilities through the kernel estimator method. In the kinematic and spatial planes, both coordinates had the same physical meaning. Now, in the photographic photometric (*R*,*B*–*R*) plane, the different meaning of the variables (magnitude and colour) requires a normalization of coordinates previous to the calculation of empirical frequency functions. This is the only difference in the treatment of the photometric plane. The normalization was done scaling the coordinate axis to get zero mean, and standard deviation equal to unity.

We defined the same inner circle and corona used in previous planes. The samples found in each of these regions were treated in the normalized photometric plane, using a grid for the empirical frequency function tabulations. The clusters photometric empirical frequency function $\Psi_{\rm c}^{\rm p}$ (where 'p' stands for 'photometry') was computed from the mixed function determined in the inner circle, $\Psi_{\rm c+f}^{\rm p}$, subtracting from it the field contribution $\Psi_{\rm f}^{\rm p}$. The photometric frequency function in the corona $\Psi_{\rm f'}^{\rm p}$ was assumed again to represent the field contribution in the circle, affected only by a scale factor.

Fig. 3 displays the empirical photometric pdf's $\psi_{\rm c+f}^{\rm p}$, $\psi_{\rm f}^{\rm p}$, and $\psi_{\rm c}^{\rm p}$, resulting after normalizing their respective frequency functions. Fluctuations of the field photometric distribution induced slight irregularities in the non-field pdf in the area of redder stars. The clusters main sequence is well-defined. The sample brightness cutoff at R=15 mag corresponds to normalized magnitude $R_{\rm norm} \approx$1 mag. The behaviour of the faint end of the field pdf shows a clear tendency to exponential grow, while the non-field pdf becomes flat at $R_{\rm norm} \approx$0.5 mag.

For a star placed at grid node $\{[R_i, (B-R)_j]; i, j = 1, \cdots, N_c\}$, the photometric probability of it not being a field star is:

$$P_{\rm c}^{\rm p}[R_i, (B-R)_j] = \frac{\Psi_{\rm c+f}^{\rm p}[R_i, (B-R)_j] - \Psi_{\rm f}^{\rm p}[R_i, (B-R)_j]}{\Psi_{\rm c+f}^{\rm p}[R_i, (B-R)_j]} \quad (6)$$

4. Membership determination

4.1. Selection criteria

Individual membership probabilities were computed for the selected star sample from Eqs. 4, 5 and 6. We defined a selection parameter $P_{\rm c} = P_{\rm c}^{\rm k} P_{\rm c}^{\rm s} P_{\rm c}^{\rm p}$. This parameter could be interpreted as the probability of a star not being a field star if the variables were independent, but they are not. However, the values of a

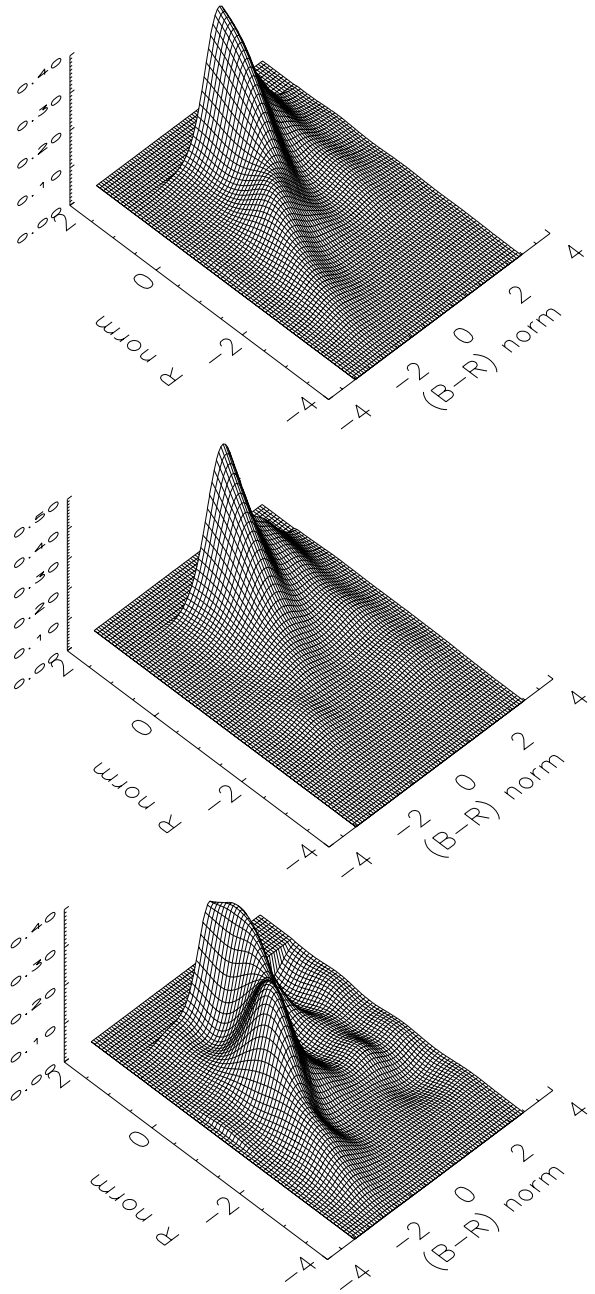

Fig. 3. Photometric empirical pdf's. Top: $\psi^{\rm p}_{\rm c+f}$ (mixed sample) from the inner circle of radius $25'$. Center: $\psi^{\rm p}_{\rm f}$ (field population) from the corona between $30'$ and $45'$. Bottom: $\psi^{\rm k}_{\rm c}$ (non-field, or clusters population). Axis are in normalized coordinates. Note that the magnitude axis is reversed respect to the usual orientation

probability computed in the 6-dimensional space are correlated with the values of $P^{\rm k}_{\rm c}$, $P^{\rm s}_{\rm c}$ and $P^{\rm p}_{\rm c}$ and, thus, $P_{\rm c}$ is related to the cluster membership probability.

The selection parameter was not calculated for the stars lying in the kinematic plane zones of low cluster density, where $\psi^{\rm k}_{\rm c} < 3\gamma$ (Sect. 3.1). From the integrated volume of the cluster kinematic frequency function $\Psi^{\rm k}_{\rm c}$ in the high cluster density areas ($\psi^{\rm k}_{\rm c} > 3\gamma$), we obtain an expected number of cluster members equal to 158 stars. The integration of the field kinematic frequency function $\Psi^{\rm k}_{\rm f}$ in the same areas predicts a field population of 139 stars. The clusters/field population ratio, for the selected sample with computed probabilities, is only 1.12, what gives an idea of the poorness of the clusters.

The number of cluster members was tested performing a set of computations for different values of the parameters involved in the empirical determination of frequency functions: the spatial center of the studied area, the radii of the cluster circle (ρ) and the corona (ρ_o and ρ_1), the smoothing parameter (h) and the noise threshold ($n\gamma$) in the kinematic plane. From this test we conclude that the predicted number of members for the cluster populations is determined with an uncertainty of 12%.

As seen in Fig. 1, the clear separation of the two clusters in the kinematic plane suggests an obvious criterion for assigning non-field stars to NGC 1750 or NGC 1758, according to their distances from the maxima of $\Psi^{\rm k}_{\rm c}$. From this classification criterion, and taking into account the uncertainty level mentioned above, the number of expected members (from the integration of $\Psi^{\rm k}_{\rm c}$) is 92 ± 11 for NGC 1750, and 66 ± 8 for NGC 1758. The cluster/field population ratio is 1.19 for NGC 1750, and 1.08 for NGC 1758. The selected sample was sorted in order of increasing selection parameter $P_{\rm c}$. From the sorted list, the first 92 stars closer to the $\Psi^{\rm k}_{\rm c}$ maximum of NGC 1750 than to the maximum of NGC 1758 were assigned to the first cluster. In an analogous way, the first 66 stars closer to NGC 1758 maximum than to NGC 1750 maximum were assigned to NGC 1758.

Bright stars lacking photographic photometry due to saturation were assigned $P^{\rm p}_{\rm c} = 0$ and, thus, $P_{\rm c} = 0$. These stars were checked individually, searching for high $P^{\rm k}_{\rm c}$ and $P^{\rm s}_{\rm c}$ values. The star number 46326 ($V = 8.4$ mag) has high spatial and kinematic probabilities of belonging to NGC 1750. It was added to NGC 1750 list, and the star of NGC 1750 with the lowest classification parameter was dropped.

Probabilistic methods for assigning membership always imply a certain degree of contamination by field stars and some amount of non-identified members. Our selection method does not provide an internal estimation of its efficiency. However, the nature of the data allows to apply some *external*, physical criteria, to evaluate the degree of field contamination in the resulting lists of selected stars. These lists were used to perform preliminary colour excess, distance and age calculations as described in Sects. 5.2 and 5.3. The resulting isochrones for single stars and for equal-mass binaries were compared with the star positions on the colour-magnitude diagrams. Those stars whose location is not compatible with the isochrones, taking into account twice the individual photometric error boxes, were considered field stars and were dropped from the selection. In this way, we found 13 field stars in the selection done for NGC 1750, and 9 in that for NGC 1758. So, the final accepted lists of members contain 79 stars for NGC 1750 and 57 stars for NGC 1758. Since the predicted number of members was 92 and 66, we evaluate that the selection of individual member stars has an efficiency upper bound of 86%. Of course, this figure is not related only to the method itself, but also to the specific properties of the studied

Table 1. NGC 1750 members. Columns contain: identification number from Paper II, individual membership probabilities in the kinematic (P_c^k), spatial (P_c^s) and photometric (P_c^p) planes, equatorial coordinates for the epoch 1994.9, equinox J2000.0 and ICRS reference system, *BVR* photometry, source of photometry ('C' for CCD, 'P' for photographic), cross-identifications and notes. Cross identifications are given in two subcolumns: with a general catalogue and with a previous study of the area. For the general catalogue, the identifier is taken (in order of preference) from BD, HD or Tycho. For the previous study, the identifier is taken (in order of preference) from Cuffey (1937), SČM or Paper I (GJTR)

star	P_c^k	P_c^s	P_c^p	α ($^h\,^m\,^s$)	δ ($^\circ\,'\,''$)	B	V	R	source	cross-identifications		notes
56573	0.57	0.31	0.76	5 3 04.582	+23 37 37.20	13.54	12.91	12.60	C		GJTR 723	a
51577	0.63	0.40	0.51	5 3 05.724	+23 44 01.33	14.61	13.86	13.38	C		GJTR 741	
52941	0.68	0.44	0.52	5 3 12.457	+23 42 07.68	14.54	13.71	13.54	C		GJTR 853	
52277	0.64	0.44	0.81	5 3 13.775	+23 42 59.26	12.58	12.10	11.79	C		Cuf 18	
46326	0.46	0.31		5 3 17.292	+23 49 17.37	8.61	8.41	8.21	C	BD+23 815	Cuf 23	b
49398	0.54	0.38	0.81	5 3 19.069	+23 46 38.85	12.98	12.42	12.06	C		GJTR 952	
36665	0.67	0.20	0.87	5 3 20.867	+24 01 35.39	12.76	12.31	12.06	P			
51802	0.63	0.46	0.74	5 3 22.527	+23 43 32.44	11.69	11.31	11.11	C		Cuf 19	
47381	0.55	0.35	0.88	5 3 23.288	+23 48 53.33	10.85	10.62	10.43	C	TYC 1845 2341	Cuf 24	
52103	0.44	0.47	0.70	5 3 25.533	+23 43 12.02	13.35	12.63	12.23	C		GJTR 1111	
56264	0.58	0.44	0.39	5 3 31.122	+23 38 02.24	15.45	14.54	14.01	C		GJTR 1241	
54959	0.58	0.48	0.83	5 3 31.718	+23 39 25.72	10.83	10.49	10.31	C	BD+23 817	Cuf 13	
53689	0.65	0.50	0.94	5 3 32.590	+23 40 46.94	9.85	9.60	9.46	C	BD+23 819	Cuf 14	
52764	0.64	0.51	0.88	5 3 37.945	+23 42 01.84	13.31	12.71	12.39	C		GJTR 1406	
52762	0.58	0.50	0.88	5 3 38.240	+23 42 15.23	13.37	12.75	12.41	C		GJTR 1420	
51560	0.69	0.50	0.92	5 3 38.561	+23 43 49.72	11.02	10.69	10.50	C	TYC 1845 1628	Cuf 21	
51618	0.65	0.51	0.51	5 3 43.124	+23 43 53.44	14.97	14.11	13.61	C		GJTR 1523	
48267	0.57	0.45	0.79	5 3 45.508	+23 47 53.69	12.00	11.63	11.44	C		Cuf 26	
48731	0.46	0.46	0.79	5 3 45.532	+23 47 17.18	12.12	11.71	11.50	C		Cuf 25	
57777	0.69	0.44	0.85	5 3 45.895	+23 35 51.66	10.90	10.63	10.43	C	HD 285126	Cuf 8	
48480	0.54	0.47	0.86	5 3 47.919	+23 47 38.64	12.69	12.23	12.00	C		Cuf 27	
54631	0.67	0.54	0.28	5 3 48.403	+23 39 58.82	15.33	14.39	13.84	C		GJTR 1639	
44008	0.60	0.43	0.73	5 3 49.037	+23 52 33.98	13.70	13.06	12.69	C		GJTR 1648	
58050	0.53	0.46	0.59	5 3 50.680	+23 35 36.68	13.11	12.50	12.10	C		GJTR 1699	
59844	0.60	0.37	0.52	5 3 51.376	+23 33 25.69	14.37	13.62	13.16	C		GJTR 1716	
56824	0.42	0.52	0.84	5 3 54.124	+23 37 09.09	12.70	12.22	11.92	C		GJTR 1779	
40874	0.67	0.43	0.92	5 3 54.928	+23 56 05.55	10.32	10.06	9.94	C	BD+23 823	Cuf 119	c
53529	0.50	0.56	0.76	5 3 57.643	+23 41 06.34	11.72	11.36	11.17	C	TYC 1845 3241	Cuf 31	
42040	0.50	0.49	0.85	5 3 59.675	+23 54 55.63	13.14	12.62	12.30	C		GJTR 1936	
55681	0.48	0.56	0.81	5 3 59.746	+23 38 46.80	13.52	12.85	12.51	C		GJTR 1947	
50817	0.68	0.56	0.73	5 3 59.779	+23 44 44.24	11.24	10.92	10.76	C	TYC 1845 2730	Cuf 29	
58193	0.55	0.49	0.52	5 3 59.810	+23 35 28.65	14.75	13.95	13.46	C		GJTR 1950	
49416	0.49	0.55	0.76	5 4 00.816	+23 46 24.07	11.57	11.25	11.10	C	TYC 1845 2079	Cuf 28	
50818	0.68	0.56	0.69	5 4 00.839	+23 44 45.06	13.32	12.74	12.44	C		GJTR 1974	
40992	0.63	0.47	0.47	5 4 03.808	+23 56 12.39	15.02	14.21	13.75	P			
61873	0.71	0.29	0.72	5 4 05.726	+23 30 59.30	13.87	13.22	12.82	C		GJTR 2090	
38367	0.71	0.37	0.46	5 4 08.971	+23 59 18.39	14.91	14.00	13.56	P			
52104	0.52	0.60	0.56	5 4 10.992	+23 43 07.48	14.70	13.94	13.46	C		GJTR 2198	
54271	0.58	0.59	0.84	5 4 12.425	+23 40 06.48	12.59	12.16	11.90	C		Cuf 34	
55285	0.58	0.59	0.93	5 4 13.964	+23 38 50.85	10.19	9.89	9.68	C	HD 285122	Cuf 32	
52885	0.58	0.61	0.52	5 4 15.404	+23 42 04.27	14.79	14.05	13.57	C		GJTR 2298	
53086	0.59	0.61	0.68	5 4 15.974	+23 41 42.32	11.58	11.27	11.05	C	HD 285123	Cuf 33	
37775	0.67	0.34	0.84	5 4 17.729	+24 00 02.21	12.57	12.16	11.90	P			
57181	0.48	0.55	0.74	5 4 18.817	+23 36 39.71	14.04	13.36	12.94	C		GJTR 2366	
48269	0.69	0.65	0.32	5 4 19.127	+23 47 55.07	15.09	14.19	13.62	C		Cuf 339	
39116	0.57	0.40	0.86	5 4 20.296	+23 58 15.39	12.76	12.20	12.04	P			
50179	0.46	0.65	0.63	5 4 21.425	+23 45 26.17	11.69	11.26	11.03	C	TYC 1845 2938	Cuf 39	
36686	0.62	0.28	0.68	5 4 22.621	+24 01 24.79	11.84	11.40	11.17	P			
50979	0.57	0.65	0.38	5 4 23.247	+23 44 36.76	15.28	14.39	13.85	C		GJTR 2470	
54327	0.68	0.60	0.36	5 4 26.187	+23 40 03.02	15.16	14.33	13.82	C		GJTR 2542	
48072	0.62	0.69	0.29	5 4 29.428	+23 48 06.64	15.36	14.44	13.86	C		Cuf 481	
53923	0.57	0.61	0.79	5 4 31.318	+23 40 32.98	12.53	12.02	11.72	C		Cuf 35	
52124	0.59	0.66	0.35	5 4 31.620	+23 43 03.37	15.55	14.67	14.11	C		GJTR 2671	
57615	0.62	0.49	0.83	5 4 32.999	+23 35 57.70	11.09	10.77	10.60	C	TYC 1845 2656	Cuf 4	
50542	0.58	0.68	0.84	5 4 34.329	+23 45 00.60	12.55	12.11	11.90	C		Cuf 38	d
58905	0.57	0.44	0.63	5 4 35.514	+23 34 31.13	13.84	13.14	12.67	P			
52173	0.48	0.66	0.83	5 4 36.127	+23 42 56.80	12.83	12.33	12.03	C		Cuf 36	d
46151	0.43	0.69	0.77	5 4 36.530	+23 49 44.87	11.17	10.76	10.51	C	HD 285116	Cuf 44	
54608	0.62	0.59	0.57	5 4 39.084	+23 39 51.77	14.58	13.73	13.27	C		GJTR 2837	
48184	0.58	0.70	0.72	5 4 39.885	+23 47 34.58	13.98	13.25	12.81	C		Cuf 498	d
49419	0.58	0.70	0.55	5 4 42.475	+23 46 26.50	14.44	13.64	13.21	C		Cuf 546	c
52848	0.55	0.63	0.28	5 4 44.608	+23 42 03.98	15.88	14.96	14.46	C		GJTR 2961	

objects, and we expect the method to be more efficient when applied to densely populated clusters.

Fig. 4 represents the proper motion of the stars finally classified in each group (field, NGC 1750 and NGC 1758). The lists of members are displayed in Tables 1 (79 stars) and 2 (57 stars). These tables contain positional and photometric information, as well as the individual membership probabilities computed in the three observational planes. The epoch of the equatorial coordinates is that of the master plate of Paper II (1994.9), the equinox is J2000.0, and the reference system is ICRS. The stars are sorted in order of increasing right ascension. For the stars within the CCD photometric sample of Paper I, the *BVR* pho-

Table 1. (continued)

star	P_c^k	P_c^s	P_c^p	α ($^h\ ^m\ ^s$)	δ ($^\circ\ '\ ''$)	B	V	R	source	cross-identifications		notes
50438	0.54	0.68	0.80	5 4 48.470	+23 45 08.23	13.93	13.21	12.84	C		Cuf 542	
36617	0.64	0.23	0.86	5 4 49.150	+24 01 29.82	13.36	12.80	12.50	P			
60014	0.61	0.39	0.72	5 4 53.185	+23 33 00.05	13.94	13.29	12.88	P			
50225	0.57	0.64	0.87	5 4 55.999	+23 45 11.84	10.90	10.62	10.44	C	HD 285118	Cuf 51	d
60778	0.52	0.40	0.79	5 5 00.456	+23 32 09.84	13.62	13.03	12.63	P			
42682	0.57	0.46	0.49	5 5 03.104	+23 53 55.64	14.53		13.71	P			
50668	0.66	0.55	0.58	5 5 08.657	+23 44 51.59	14.57	13.80	13.36	P			
55683	0.49	0.46	0.67	5 5 09.345	+23 38 36.02	14.17	13.50	13.09	P			
47553	0.60	0.53	0.60	5 5 09.409	+23 48 36.58	14.43	13.55	13.22	P			
62363	0.49	0.37	0.83	5 5 10.534	+23 30 10.91	13.54	12.70	12.62	P			
59667	0.56	0.41	0.51	5 5 13.137	+23 33 19.52	14.71	13.85	13.41	P			
53996	0.58	0.46	0.81	5 5 13.275	+23 40 14.92	11.55	11.33	11.06	P			
57943	0.70	0.42	0.36	5 5 14.903	+23 35 34.41	15.15		13.71	P			
52809	0.65	0.44	0.85	5 5 27.501	+23 41 41.84	10.96	10.69	10.49	P	TYC 1845 2720		
50552	0.59	0.46	0.79	5 5 30.602	+23 44 52.98	13.61	12.97	12.64	P			
47835	0.56	0.41	0.60	5 5 37.402	+23 48 10.36	13.86	13.16	12.68	P			
56111	0.49	0.25	0.88	5 5 50.896	+23 37 49.10	12.90	12.47	12.24	P			

Notes:

[a] R value is photographic for this star

[b] A2e star (McCarthy & Treanor 1965)

[c] Assigned by SČM to the field

[d] Assigned by SČM to NGC 1758

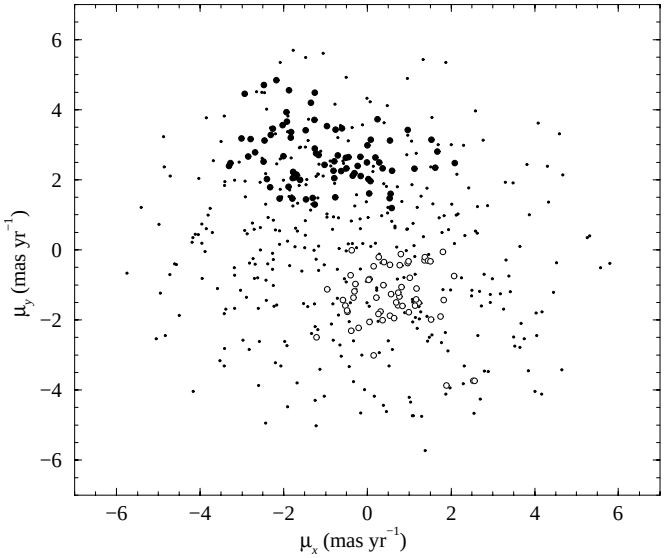

Fig. 4. Proper motion distribution of field stars (dots) and cluster members (filled circles for NGC 1750, empty circles for NGC 1758). The axis alignment is $x \leftrightarrow -\delta, y \leftrightarrow -\alpha$

tometry quoted in Tables 1 and 2 was taken from that source, because CCD photometry is more accurate than photographic photometry. For the other stars, we give photographic photometry from Paper II. None of the members is included in the Hipparcos catalogue, and 17 of them appear in the Tycho catalogue (ESA 1997). Tables 1 and 2 include, when available, cross-identifications with one general catalogue and with one previous study of the area. We refer to Paper II for a more complete table of cross-identifications.

4.2. Bright stars

The bright section of the clusters main sequences is crucial for the determination of several fundamental physical parameters of the groups, in particular the age. So, we took great care in ensuring that bright star classification was as complete as possible from the data at our disposal.

Bright members could be excluded from classification for two reasons. The first was the absence of data which did not allow the computation of the selection parameter for stars present in the selected sample. This case was considered in the previous section and led to the inclusion of star number 46326 (which did not have photographic photometry) as a member of NGC 1750. There were no more stars in a similar situation.

The second reason for the possible loss of bright stars was their exclusion from the selected sample. Some bright stars might be absent from the astrometric and photometric catalogue of Paper II, if they lack *both* proper motions and photographic photometry. We have checked that all PPM (Röser & Bastian 1989), TYC and HIP stars in the cluster zone are present in our catalogue. All stars from SČM and all bright ($V < 12.5$ mag) stars from Paper I are present in the astrometric and photometric photographic catalogue. We conclude that, for bright stars, the catalogue of Paper II does not overlook any star in the cluster zone. However, the information is not always complete and/or of good quality for bright stars, and this means some of them are not included in the selected sample. The exclusion of relevant stars could be due to the lack of proper motion, or to large proper motion error. This is the case of 11 stars down to $R = 12$ mag inside the cluster region.

Three of these stars (numbers 40505, 54380 and 60165) lack both CCD and photographic photometry. Star 40505 (SČM 87, Cuffey 137) has K0 spectral type according to HD catalogue, and G8 II according to SČM. Star 54380 (SČM 68, Cuffey 1) has K0 spectral type according to HD catalogue, and G5 IV according to SČM. This star is included in the Hipparcos

Table 2. NGC 1758 members. Columns contain the same information as in Table 1

star	P_c^k	P_c^s	P_c^p	α ($^h\ ^m\ ^s$)	δ ($^\circ\ '\ ''$)	B	V	R	source	cross-identifications		notes
53258	0.55	0.50	0.37	5 3 31.555	+23 41 42.22	15.65	14.83	14.32	C		GJTR 1252	
40454	0.62	0.27	0.54	5 3 35.528	+23 56 39.58	14.68	13.99	13.57	C		GJTR 1340	
49797	0.61	0.45	0.37	5 3 36.516	+23 46 10.75	15.40	14.48	13.94	C		GJTR 1374	
39209	0.42	0.42	0.64	5 4 09.657	+23 58 13.77	14.34	13.68	13.36	P			
57323	0.67	0.55	0.27	5 4 12.317	+23 36 32.33	16.46	15.34	14.69	C		GJTR 2235	
54924	0.66	0.59	0.24	5 4 12.633	+23 39 33.12	16.19	15.25	14.69	C		GJTR 2246	
40198	0.57	0.47	0.39	5 4 12.890	+23 56 53.64	15.34		13.95	P			
48478	0.63	0.63	0.40	5 4 15.537	+23 47 38.04	14.79	13.97	13.46	C		Cuf 341	
57021	0.51	0.56	0.50	5 4 15.980	+23 36 54.36	14.79	14.08	13.64	C		GJTR 2311	
29443	0.60	0.36	0.62	5 4 16.941	+24 10 21.25	13.27	12.61	12.13	P			
51234	0.54	0.63	0.38	5 4 17.191	+23 44 18.54	15.62	14.70	14.23	C		GJTR 2329	
48456	0.65	0.64	0.49	5 4 17.460	+23 47 40.03	14.80	14.07	13.60	C		Cuf 340	
57360	0.63	0.54	0.78	5 4 19.119	+23 36 21.70	12.29	11.86	11.61	C		Cuf 5	a
59526	0.37	0.45	0.75	5 4 19.396	+23 33 39.23	11.90	11.58	11.33	P		SČM 58	a
56333	0.65	0.57	0.64	5 4 22.074	+23 37 49.85	14.33	13.65	13.25	C		GJTR 2442	
44069	0.61	0.62	0.66	5 4 22.952	+23 52 14.51	11.54	11.13	10.85	C	TYC 1845 2990	Cuf 42	
55233	0.48	0.59	0.39	5 4 23.388	+23 39 07.26	15.56	14.65	14.12	C		GJTR 2479	
42481	0.64	0.56	0.84	5 4 23.628	+23 54 19.94	13.32	12.85	12.53	C		GJTR 2474	
45584	0.54	0.67	0.43	5 4 31.555	+23 50 33.85	15.22	14.37	13.89	C		Cuf 478	
50090	0.67	0.69	0.89	5 4 32.243	+23 45 35.51	13.48	12.93	12.64	C		Cuf 501	
47183	0.52	0.69	0.81	5 4 32.807	+23 49 06.53	13.46	12.85	12.49	C		Cuf 483	a
56998	0.66	0.52	0.75	5 4 32.851	+23 36 52.24	13.95	13.27	12.92	C		GJTR 2708	
44326	0.51	0.64	0.87	5 4 35.455	+23 52 02.91	13.22	12.73	12.52	C		Cuf 487	
44884	0.65	0.66	0.64	5 4 36.745	+23 51 21.91	14.06	13.31	12.86	C		Cuf 487q	
44639	0.62	0.65	0.37	5 4 38.514	+23 51 39.51	15.47	14.57	14.03	C		GJTR 2822	
51217	0.53	0.68	0.65	5 4 39.179	+23 44 10.97	12.40	11.97	11.74	C		Cuf 37	
48181	0.52	0.70	0.86	5 4 39.970	+23 47 53.17	12.84	12.28	11.99	C		Cuf 46	
46762	0.38	0.69	0.83	5 4 42.021	+23 49 16.80	13.58	12.97	12.64	C		SČM 77	
48661	0.48	0.70	0.26	5 4 42.159	+23 47 20.70	16.13	15.15	14.60	C		GJTR 2910	
44721	0.68	0.65	0.59	5 4 42.383	+23 51 32.29	14.57	13.87	13.40	C		Cuf 489	
53753	0.52	0.61	0.84	5 4 43.072	+23 40 47.05	13.30	12.79	12.52	C		GJTR 2925	
47176	0.55	0.69	0.28	5 4 43.331	+23 49 08.33	15.81	14.90	14.39	C		GJTR 2926	
46191	0.36	0.67	0.85	5 4 45.784	+23 49 48.03	12.83	12.29	12.00	C		Cuf 493	
50789	0.38	0.68	0.89	5 4 45.931	+23 44 45.04	13.01	12.53	12.30	C		Cuf 541	
47146	0.58	0.68	0.72	5 4 46.321	+23 49 00.39	12.63	12.10	11.84	C		Cuf 495	
46538	0.59	0.67	0.79	5 4 46.775	+23 49 32.60	14.02	13.39	13.02	C		Cuf 494	
47776	0.68	0.67	0.34	5 4 50.450	+23 48 26.09	15.77	14.83	14.28	C		GJTR 3076	
50221	0.67	0.67	0.81	5 4 50.473	+23 45 19.62	12.36	11.94	11.71	C		Cuf 52	
36852	0.65	0.23	0.84	5 4 51.137	+24 01 04.57	12.53	12.09	11.87	P			
46091	0.59	0.64	0.81	5 4 52.722	+23 49 54.01	13.40	12.75	12.39	C		Cuf 48	a
36473	0.66	0.21	0.73	5 4 52.812	+24 01 42.45	14.03	13.40	13.01	P			
39988	0.66	0.38	0.90	5 4 55.046	+23 56 59.29	13.29	12.85	12.63	P			
62671	0.44	0.31	0.70	5 4 56.194	+23 29 48.05	12.34	12.00	11.48	P			
50927	0.60	0.63	0.32	5 4 56.937	+23 44 35.91	15.95	15.05	14.54	C		GJTR 3164	
50669	0.64	0.62	0.83	5 5 00.111	+23 44 53.84	14.37	13.66	13.23	C		GJTR 3198	
51664	0.55	0.58	0.41	5 5 01.768	+23 43 38.32	15.36	14.54	14.06	C		GJTR 3211	
50744	0.54	0.59	0.49	5 5 03.822	+23 44 48.91	14.98	14.24	13.78	P			
40895	0.54	0.37	0.78	5 5 05.077	+23 56 04.36	12.26	11.89	11.61	P			
49125	0.46	0.58	0.39	5 5 05.102	+23 46 42.47	15.12	14.23	13.70	P			
49751	0.53	0.54	0.88	5 5 09.733	+23 45 57.76	13.14	12.64	12.33	P			
44584	0.57	0.38	0.48	5 5 22.790	+23 51 36.70	14.57	13.69	13.22	P			
44175	0.62	0.33	0.47	5 5 32.588	+23 52 08.47	15.07	14.22	13.93	P			
53133	0.51	0.43	0.44	5 5 33.432	+23 41 33.08	15.16		14.00	P			
47743	0.58	0.42	0.82	5 5 34.395	+23 48 15.42	12.41	12.06	11.80	P			
50256	0.58	0.44	0.36	5 5 40.683	+23 45 15.23	15.64	14.71	14.30	P			
41079	0.56	0.22	0.87	5 5 41.921	+23 55 47.57	13.35	12.74	12.51	P			
47653	0.63	0.38	0.89	5 5 43.497	+23 48 23.46	13.43	12.90	12.67	P			

Notes:

[a] Assigned by SČM to the field

catalogue as HIP 23606, with an absolute trigonometric parallax of $\pi = 4.75 \pm 1.09$ mas, equivalent to a distance of 171-273 pc. Finally, star number 60165 (SČM 60, Cuffey 7) is quoted as K5 spectral type by HD and as K4 II-III by SČM. From their spectral types and apparent visual magnitudes, none of these stars can belong to the clusters, but rather are foreground objects.

The remaining 8 stars have large proper motion errors, but photographic or CCD photometric data are available for them. These are stars numbers 30153, 39438, 41799, 46570, 49525, 54871 55058 and 58932. The magnitude and colour of three of them are clearly incompatible with membership, since they are late type too bright stars: 30153, 58932 and 41799. Star 39438 is photometrically compatible, but the proper motion of this star along the x axis has small error ($\sigma_{\mu x} = 0.76$ mas yr^{-1}) and it is incompatible with both clusters. The other four stars are brighter and photometrically compatible with membership. Three of them are spatially located in NGC 1750 area and, at the same time, their proper motion values and errors, in spite of their inaccuracy, make it unlikely that they are members of NGC 1758. These stars are 49525 (SČM 52, Cuffey 22), 54871 (SČM 42, Cuffey 23) and 55058 (SČM 48, Cuffey 12). SČM classified them as NGC 1750 members. Star 46570 (SČM 79, Cuffey 47) is located in the maximum stellar density zone of NGC 1758, and its photometry places it among other bright

members of this cluster. Its proper motion and proper motion errors allow us to discard the membership of this star to NGC 1750. SČM classified it as being a member of NGC 1758.

More accurate proper motions would be needed for these four stars in order to confirm their membership. We did not include them in our member lists, although we took into account their existence, checking the effect of including them when computing the physical parameters of the clusters. These four stars are referred to as 'possible members' from now on. Positional and photometric information on these stars is displayed in Table 3.

It still seems convenient to comment on some additional bright stars, in terms of their location on the colour-magnitude diagrams or other special features:

- Star 46326 (BD+23° 815, SČM 43), the brightest member of NGC 1750, is an A2e star (McCarthy & Treanor 1965), which might have been shifted in the colour-magnitude diagram from the location that it would have had if it was a normal star. It is necessary to take this point into account when drawing conclusions about this cluster.
- Red stars 35542 (TYC 1845 2818) and 64305 have proper motions compatible with membership to NGC 1758, and they are well placed in the colour-magnitude diagram for being considered as red giants belonging to this group. But their spatial positions are very far away from NGC 1758 center, leading to very low P_c^s values. These stars were classified into the field population and this is probably correct, although more detailed individual observations would be welcome in order to confirm this point.
- Star 55058, a possible member of NGC 1750, has a bright close companion (55059, SČM 46, V=9.97 mag from Paper I) at a distance of $20''$, classified as a field star by SČM and by us. This pair was included as a double star in AG Catalog and appears in the *Washington Visual Double Star Catalog* (Worley & Douglas 1984) as entry WDS 4585+2331. It is worth noticing that this pair cannot be a binary star belonging to the cluster, and most probably (if the membership of star 55058 is confirmed) they constitute an optical pair.

To finish our discussion of bright stars, we briefly compare our membership determination with SČM's results. SČM assigned 14 stars to NGC 1750 and 16 to NGC 1758. From these, stars 49525, 54871, 55058 and 46570 (SČM 52, 42, 48 and 79) have large proper motion errors and, as commented above, they are not included in our selected sample. From the remaining 26 SČM non-field stars, 21 of them are classified as non-field by us, and 5 are found to be field stars (56551, 48916, 45281, 47149 and 47443, SČM numbers 49, 75, 78, 81 and 92). Furthermore, 6 stars assigned to the field population by SČM are included in the cluster population in our study (they are labelled in Tables 1 and 2).

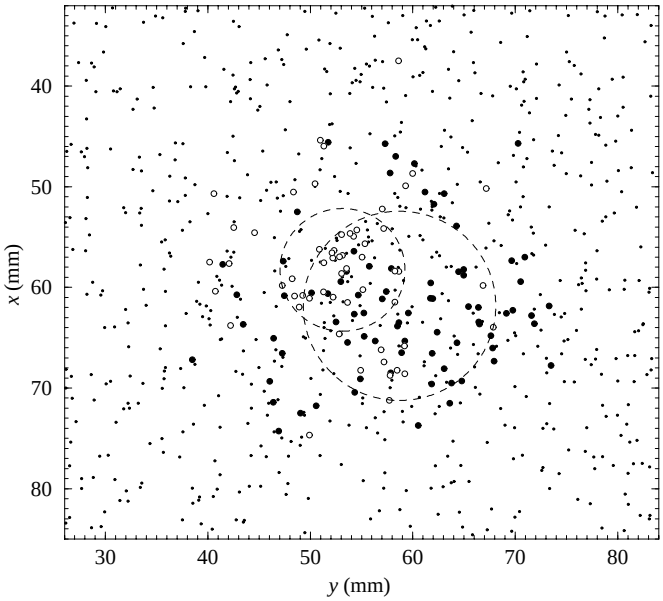

Fig. 5. Projected (2D) spatial distribution of field stars (dots) and cluster members (filled circles for NGC 1750, and empty circles for NGC 1758). Dashed circles centered at cluster average positions contain half the total number of member stars for each cluster. Circle radii are $10.2'$ for NGC 1750 and $6.6'$ for NGC 1758. North is up, East is left. The scale is $65.25''$ mm^{-1}

5. Physical parameters of the clusters

5.1. Spatial parameters: positions, sizes and density profiles

Fig. 5 displays the projected (2D) spatial distribution of the stars classified as field and non-field. NGC 1758 shows a dense core and a disperse corona while the central concentration of NGC 1750 is less outstanding. It should be remembered that the assignation of non-field stars to NGC 1750 or NGC 1758 was made on the sole basis of their proper motions.

The position of the cluster centers were computed by averaging the coordinates of member stars. The resulting equatorial positions (epoch 1994.9, equinox J2000.0) are $5^h4.3^m + 23°44'$ for NGC 1750, and $5^h4.7^m + 23°48'$ for NGC 1758. A way of estimating the cluster sizes is to determine the radius of the circle that contains half the total number of cluster members. These radii are found to be $10.2'$ and $6.6'$ for NGC 1750 and NGC 1758, respectively. These values would be underestimations of the true half-sample radii, if mass segregation was present in the clusters.

Our method for computing probabilities in the spatial plane did not imply the assumption of any definite model for the cluster stellar density profiles. This allows us to analyze the spatial distribution of cluster members in order to retrieve this information. We plotted the cluster profiles by counting the stars found in successive annuli centered on the cluster positions, and the result is shown in Fig. 6, where error bars are computed assuming a Poisson error distribution for the number of stars counted in each annulus.

Table 3. Possible bright members, not included in our selected sample. The first nine columns contain identification number, positional and photometric data and cross-identifications, and have the same meaning as in Tables 1 and 2. The last column displays the cluster to which each star might belong

star	α ($^{\rm h}$ $^{\rm m}$ $^{\rm s}$)	δ ($^\circ$ $'$ $''$)	B	V	R	source	cross-identifications		NGC
46570	5 4 44.844	+23 49 25.92	11.96	11.59	11.38	C		Cuf 47	1758
49525	5 3 50.501	+23 46 05.98	9.83	9.48	9.32	C	BD+23 822	Cuf 22	1750
54871	5 3 14.764	+23 39 22.39	9.46	9.20		C	BD+23 814	Cuf 15	1750
55058	5 3 38.646	+23 39 06.72	9.77	9.44	9.28	C	BD+23 821	Cuf 12	1750

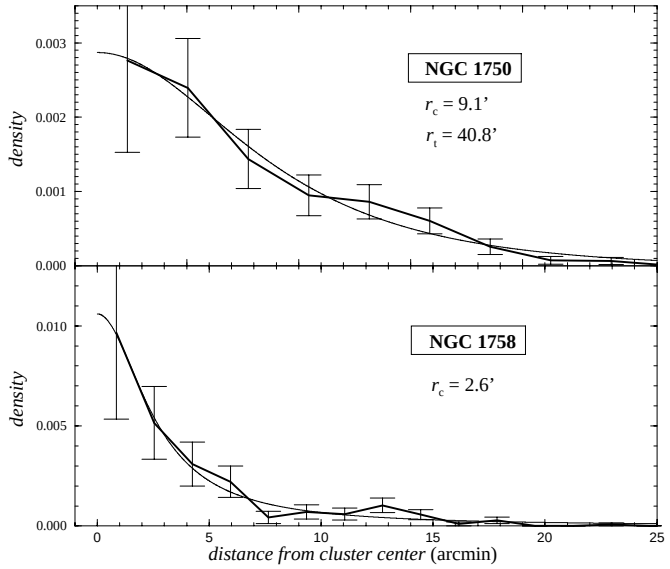

Fig. 6. Spatial stellar density profiles for NGC 1750 (top) and NGC 1758 (bottom). Density is measured in units of fraction of the total sample per square arcmin. Error bars assume poisson statistics. Thin lines plot the best fits to King's profiles

We fitted King's (1962) functions to the empirical density profiles:

$$\rho(r) = \rho_o \left[\frac{1}{\sqrt{1+\left(\frac{r}{r_{\rm c}}\right)^2}} - \frac{1}{\sqrt{1+\left(\frac{r_{\rm t}}{r_{\rm c}}\right)^2}} \right]^2$$

with $\rho(r) = 0 \quad \forall \quad r > r_{\rm t}$. Parameters $r_{\rm c}$ and $r_{\rm t}$ are called 'core radius' and 'tidal radius', respectively. The core radius is equal to the distance from the center at which the local density of stars is half the maximum, while the tidal radius marks the distance at which the model predicts the stellar density of the cluster is equal to zero.

The fit to NGC 1750 is good, with the resulting parameters $r_{\rm c} = 9.1'$, $r_{\rm t} = 40.8'$. For NGC 1758, a King's profile seems not to be the best model: the fitting procedure diverges, leading to the minimum residuals when $r_{\rm c} = 2.6', r_{\rm t} \to \infty$. The fitted profiles are overplotted in Fig. 6. The core radius of NGC 1750 is very similar to the half-sample radius found above. The core radius of NGC 1758 is clearly less than its half-sample radius, indicating the strong central concentration of this object. No significant mass segregation is found in the clusters down to the magnitude limit reached in our selection of members.

The addition of the four bright possible members (Sect. 4.2, Table 3) do not alter significantly any of the parameters determined in this section.

Table 4. Strömgren photoelectric data for 11 stars in the area of NGC 1750 and NGC 1758. n is the number of independent measurements. For cross-identifications, refer to Tables 1, 2 and 3

star	V	*b–y*	m_1	c_1	β	n	*E*(*b–y*)
46151	10.802	0.274	0.080	1.138	2.875	2	0.249
46326	8.505	0.208	-0.005	0.144	2.559	2	0.296
49525	9.490	0.238	0.028	0.747	2.755	2	0.280
50225	10.652	0.180	0.094	0.931	2.762	2	0.213
53689	9.652	0.242	0.006	0.558	2.734	2	0.302
54871	9.280	0.220	0.024	0.654	2.736	2	0.267
54959	10.524	0.229	0.063	0.856	2.921	2	0.268
55058	9.275	0.239	-0.007	0.832	2.749	2	0.279
55285	9.874	0.244	0.020	0.793	2.736	2	0.285
57615	10.828	0.199	0.092	0.943	2.776	2	0.231
57777	10.654	0.230	-0.006	0.842	2.806	2	0.269

5.2. Absorption and colour excess

To analyze the photometric data further, it is necessary to determine the absorption as accurately as possible. The studied area lies in the direction of Taurus dark clouds. As shown by SČM (see Fig. 1 of their paper), these clouds are quite close to the Sun (about 200 pc), and the interstellar medium is very transparent beyond them, which means that the absorption does not grow with increasing distance. For this reason, we do not expect to find significant differences in colour excess between the clusters, and, also, background field stars should be reddened by the same amount as our stellar groups. This circumstance is seen in the Johnson colour-colour diagram displayed in Paper I.

Due to the multiple reddening solutions in the (*U–B,B–V*) plane (Paper I), in the present paper we estimated the absorption from Strömgren photoelectric observations which we carried out, and from the Vilnius measurements by SČM.

Eleven bright stars were observed in November 1996 using the 90 cm telescope of Instituto de Astrofísica de Andalucía at Sierra Nevada Observatory (Granada, Spain). The telescope was equipped with a multichannel photoelectric photometer and standard Strömgren-Crawford filters. The data were reduced as described in Figueras et al. (1991). The resulting photometry

was analyzed as described in Masana (1994) in order to derive *E*(*b*–*y*) values. The data are shown in Table 4.

The 11 stars observed in the Strömgren system are spread over the whole cluster area, and all are included in SČM's sample. Eight stars were classified by us as cluster members, while the other 3 are possible members (Table 3). If we accept that all 11 stars belong to the non-field population, the resulting average colour excess is $\overline{E(b-y)} = 0.27 \pm 0.03$ mag. This value can be compared with the colour excess determinations made by SČM for the same 11 stars: $\overline{E(Y-V)} = 0.28 \pm 0.02$ mag. Following Straižys (1992), $E(b-y) = 0.99E(Y-V)$ and both colour excess determinations are in perfect agreement.

The value found from these 11 stars could be affected by small-number statistics and by intrinsic fluctuations of the absorption in the observed area (McCuskey 1941). Given the agreement between our Strömgren colour excess with that derived from SČM data, we admit as true value for the clusters colour excess that derived from *E*(*Y*–*V*) measurements for all the stars from the SČM sample classified as being members by us. This sample comprises 25 stars with determined *E*(*Y*–*V*) (15 NGC 1750 members and 10 NGC 1758 members). The resulting colour excess value is compatible with that found from the previous subset of 11 stars: $\overline{E(Y-V)} = 0.26 \pm 0.05$ mag. No significant difference was found between the mean colour excess derived from NGC 1750 ($\overline{E(Y-V)} = 0.27 \pm 0.05$) and NGC 1758 ($\overline{E(Y-V)} = 0.24 \pm 0.06$) members separately.

Straižys (1992) and Straižys et al. (1992b) give the transformation coefficients: $E(B-V) = 1.325E(Y-V)$; $A_v/E(B-V) = 3.15$. So, the Johnson colour excess for both clusters is found to be $\overline{E(B-V)} = 0.34 \pm 0.07$ mag, and the corresponding absorption value is $\overline{A_v} = 1.1 \pm 0.2$ mag.

5.3. Distance and age determinations

Distance determinations were performed by fitting a zero age main sequence (ZAMS) calibrations to the faint, non-evolved section for the observed cluster main sequences. We used the empirical ZAMS calibration by Mermilliod (1981) and the solar metallicity ZAMS by Schaller et al. (1992), constructed from theoretical evolutionary models. The calibrations were shifted to take into account the absorption and colour excess determined for the clusters in the previous section. Differences between ZAMS calibrations lead to different distance modulus determinations. Since distance modulus affects luminosity and mass calculations, this fact should be kept in mind when interpreting the results. A systematic difference of 0.2 mag was found between the two ZAMS used, being brighter that from Mermilliod. For the sake of consistency, because the models by Schaller et al. (1992) were used for age determinations, from now on we use the distance modulus values derived using the ZAMS of these authors.

The distance modulus values obtained were 9.0 mag for NGC 1750, and 9.4 mag for NGC 1758. This implies cluster distances of 630 pc and 760 pc, respectively. The half-sample radii computed in Sect. 5.1 correspond, at the clusters distances, to 1.9 pc and 1.5 pc for NGC 1750 and NGC 1758, respectively.

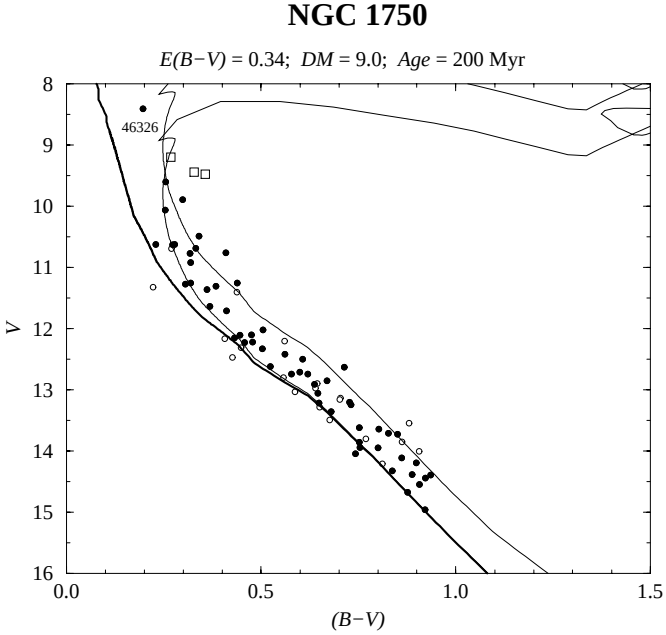

Fig. 7. NGC 1750 distance and age determination. Filled circles represent members with CCD photometry. Open circles correspond to members with only photographic photometric data. Overplotted lines are isochrones from the models by Schaller et al. (1992) for solar metallicity. Bold line is the ZAMS from the same authors. Thin lines are 200 Myr isochrones for single stars and for equal-mass double stars ($\Delta V = 0.753$ mag). The brightest member, 46326, is an A2e star. Squares represent the possible members

The fact that they are 130 pc apart is the first indication that NGC 1750 and NGC 1758 do not constitute a gravitationally bounded, binary system. If we ignore the (unknown) radial motion, we can compute a lower bound for the modulus of the relative velocity transforming the relative proper motion to linear units. The resulting relative velocity between the clusters is 13.5 km s^{-1}.

Ages were determined through isochrone fit in the (*B*–*V*,*V*) colour-magnitude diagram, following Meynet et al. (1993) and using the same isochrone set, that of Schaller et al. (1992) for solar metallicity. Lacking specific metallicity determinations for the clusters, the adoption of [Fe/H]=0 seems the obvious choice. Assuming a metallicity value based on the cluster positions in the Galaxy would require a better knowledge of the change of this parameter with galactocentric distance, a controversial subject not yet clarified (Cameron 1985, Lyngå 1982, Janes et al. 1988, Lennon et al. 1990, Twarog et al. 1997).

The low stellar density in the upper part of the main sequences is the main drawback for age determination in these clusters. The low intrinsic accuracy of photographic photometry adds to this, although this circumstance is somewhat compensated for by the fact that most cluster members have also CCD photometry. Stars with CCD photometry were given preference when performing the isochrone fits. We discarded the application of an automated fit of the kind proposed by Flannery & Johnson (1982), because these methods mean the isochrones pass through the center of the fitted samples, ignoring both

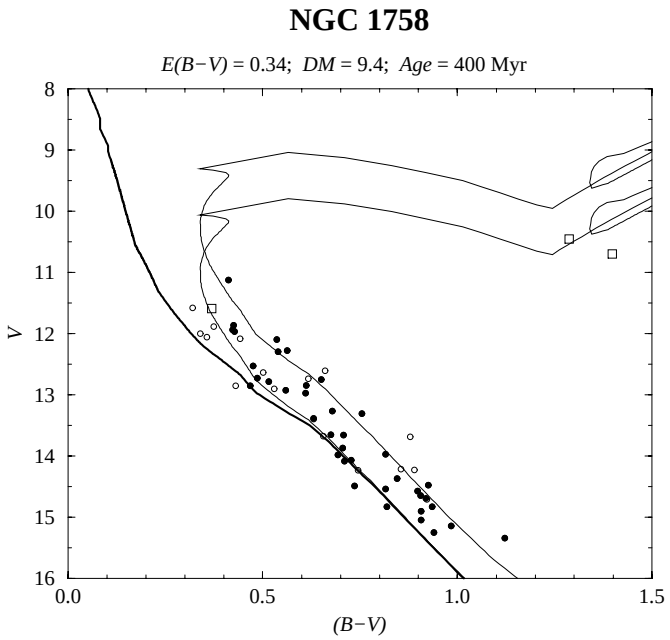

Fig. 8. NGC 1758 distance and age determination. Filled circles represent members with CCD photometry. Open circles correspond to members with only photographic photometric data. Overplotted lines are isochrones from the models by Schaller et al. (1992) for solar metallicity. Bold line is the ZAMS from the same authors. Thin lines are 400 Myr isochrones for single stars and for equal-mass double stars ($\Delta V = 0.753$ mag). The open square on the left is the possible member 46570. The squares on the right are giants 35542 and 64305 (see text)

the asymmetric profile of the main sequences and the apparent widening due to non-resolved binaries.

Figs. 7 and 8 display the isochrones overplotted to the observed Johnson (*B–V*,*V*) colour-magnitude diagrams. In both graphs, filled circles represent CCD measurements, while open circles mark the stars for which only photographic photometry is available.

When the emission-line star 46326 was considered, the resulting age for the cluster NGC 1750 was 100 Myr, while all the other bright stars of the cluster remained far below the main sequence turn-off. On the other hand, an age of 300 Myr was clearly too great, meaning the bright stars remained left of the turn-off point. An age of 200 Myr reproduces the features of the observational diagram well (Fig. 7) and keeps most bright stars with CCD photometry inside the region between the single-star isochrone and the equal mass binary star isochrone ($\Delta V = 0.753$ mag). We deduce an age of 200 ± 50 Myr for NGC 1750.

An isochrone aged 200 Myr does not reproduce the position of the turn-off point for NGC 1758. So, we can assert that both clusters have different ages, with NGC 1758 being clearly older than NGC 1750. If we fit an isochrone using only the stars with CCD photometry, we obtain an age of 500 Myr, which would be compatible with the membership of red giant candidates 35542 and 64305, classified as field stars but having proper motions compatible with NGC 1758 (Sect. 4.2). However, the 500 Myr isochrone leaves four bright members (40895, 47743, 59526 and 62671) and the possible member 46570 (Sect. 4.2) left of the turn-off point. The presence of these five bright stars in the same small area of the colour-magnitude diagram suggests they should be taken into account and, so, we placed our best guess of NGC 1758 age at 400 ± 100 Myr (Fig. 8), keeping in mind the uncertainties involved in this case. The sparseness of NGC 1758 could explain why none of its massive members were caught in the brief red giant evolutionary stage.

The fact that the cluster ages were found to be significantly different confirms that they cannot constitute a binary system.

5.4. Luminosity functions

The clusters integrated apparent visual magnitudes are V=6.82 mag for NGC 1750 and V=8.54 mag for NGC 1758. If possible members (Sect. 4.2) are included, the resulting integrated magnitudes are V=6.55 mag and V=8.47 mag, respectively.

An understanding of the luminosity functions of open clusters is one of the main sources for the investigation of the initial mass function. As our clusters are sparse and poor, the determination of their luminosity functions suffers from small number statistics and is restricted to relatively bright limiting magnitudes due to field contamination. Despite this, the observed luminosity functions show several features that make them worth studying further.

Fig. 9 displays the luminosity functions for NGC 1750 and NGC 1758, in absolute visual magnitude bins of 0.5 mag. Error bars in these diagrams assume poissonian statistics. The dashed lines show the luminosity functions obtained if the possible members (Table 3) are included. The histograms were built using the photometry quoted in Tables 1, 2 and 3.

An interesting feature present in both diagrams is the local maximum found around $M_v \approx 2.5$ mag. This detail is significant and most probably real. A similar characteristic has been found in a considerable fraction of open cluster luminosity functions in young as well as in intermediate and old objects. In all cases the dip in the luminosity function is placed around $M_v = 2.5 - 3.0$ mag. Several examples (taken from Wilner & Lada 1991, Phelps & Janes 1993, Vázquez et al. 1997, Kozhurina-Platais et al. 1995, Francic 1989) are the clusters: NGC 2362 (7 Myr), NGC 457 (10 Myr), Cr 272 (13 Myr), NGC 103 (20 Myr), NGC 659 (22 Myr), Tr 1 (27 Myr), M 25 (89 Myr), NGC 752 (250 Myr), NGC 1528 (400 Myr), NGC 6633 (800 Myr), NGC 3680 (1900 Myr).

In the case of NGC 1758, the luminosity function dip is followed by a relative gap, a feature also found in several other clusters. Furthermore, the luminosity function of NGC 1750 has a pronounced gap around $V \approx 11.5$ mag ($M_v \approx 1.5$ mag). This gap is related to the abrupt onset of convection in late A-early F stars (Böhm-Vitense & Canterna 1974, Jasniewicz 1984).

Neither of our two cluster luminosity functions shows any tendency to exponential grow at the faint end, a fact that is to be expected from the shape of the function ψ_c^p (Sect. 3.3). This indicates that the luminosity functions might be flat for faint

Table 5. Main characteristics of NGC 1750 and NGC 1758

Parameter	NGC 1750	NGC 1758
members identified ($R \leq 15$ mag)[a]	79	57
center coordinates	$\alpha = 5^{\rm h}4.3^{\rm m}, \delta = +23^\circ 44'$	$\alpha = 5^{\rm h}4.7^{\rm m}, \delta = +23^\circ 48'$
$\mu_\alpha \cos\delta$ (ICRS) [mas yr^{-1}]	–3.0	+0.7
μ_δ (ICRS) [mas yr^{-1}]	–6.0	–8.1
$E(B–V)$ [mag]	0.34 ± 0.07	0.34 ± 0.07
distance [pc]	630	760
age [Myr]	200 ± 50	400 ± 100
half-sample radius [arcmin]	10.2	6.6
core radius (King's profile) [arcmin]	9.1	2.6
integrated V [mag]	6.8	8.5
morphology	poor and loose	poor, central concentration
observed mass [$M_\odot$]	145	90

Notes:
[a] For 4 additional possible members, see Sect. 4.2

magnitudes, as found for other objects, indicating that the open cluster mass function is significantly different to that of the field in the sense that it has a deficit of low mass stars (see examples of this in Leonard 1988, Francic 1989, Wilner & Lada 1991, Sagar & Cannon 1997, Kozhurina-Platais et al. 1995). The apparent fading of the luminosity functions at the fainter extremes is due to sample incompleteness. The selected sample was cut out at $R = 15$ mag, which does not imply a sharp cutoff in V, depending on the stellar colours.

Several trials have been performed with the aim of extending the luminosity functions to fainter magnitudes not on an individual star-by-star basis, but from a statistical analysis of the sample. The results, however, are unreliable due to the exponential increase of field stars. A similar situation was found by Sagar & Cannon (1997). An extension of the luminosity functions would not be reliable unless more precise photometry and proper motions are first determined.

The binary stars data from Andersen (1991) allow us to apply a mass-luminosity relation to compute the total observed masses of the clusters: 145 $M_\odot$ for NGC 1750 and 90 $M_\odot$ for NGC 1758. As it is well known, these masses are large underestimations of the clusters true masses. Given the clusters mutual distance and the lower bound computed for their relative velocity, we would need to have cluster masses bigger than those observed by a factor larger than 10^4. Such a huge underestimation is not likely, pointing to the independent character of the clusters.

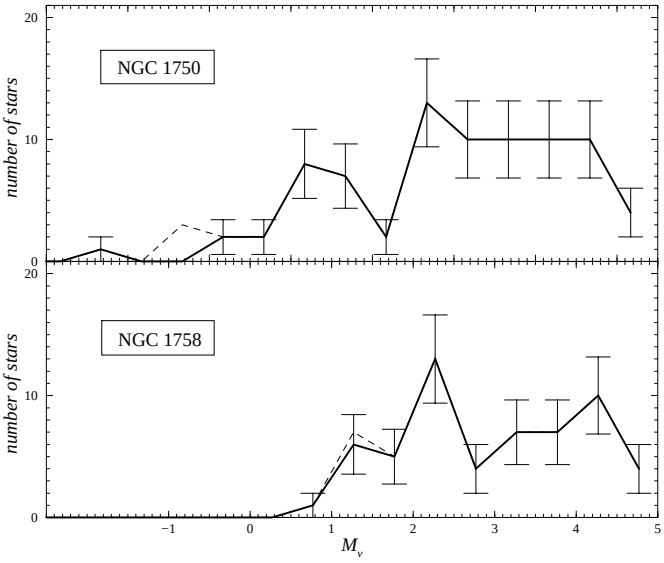

Fig. 9. Absolute luminosity functions for the clusters NGC 1750 (top) and NGC 1758 (bottom). Dashed line traces the luminosity function if possible members (Table 3) are included

6. Conclusions

A fully non-parametric method for assigning membership probabilities in open clusters was developed. This method takes into account information from three different observational planes: proper motions, positions and colour-magnitude diagram. The method was applied to astrometric and photometric data previously published by the authors in the area of the open clusters NGC 1750 and NGC 1758.

The analysis of a selected star sample allows us to conclude that the NGC entry number 1746 does not correspond to any existing object. Open clusters NGC 1750 and NGC 1758 were clearly identified and isolated. Membership probabilities down to $R = 15$ mag were computed in the three observational planes, leading to final lists of members for both clusters. The analysis of the observational data allowed positions, sizes, density profiles, colour excess, absorption, distance moduli, ages and luminosity functions for the open clusters to be determined. The main results concerning the clusters are summarized in Table 5. The luminosity functions of both clusters display an outstanding local maximum around M_v=2.5 mag.

The clusters strongly overlap in the sky, but their spatial separation (130 pc), their age difference (200 Myr) and their relative motion (modulus of the relative velocity larger than 13.5 km s^{-1}) indicate that NGC 1750 and NGC 1758 are not mutually bound, but simply overlapping clusters. Making an analogy with double stars nomenclature, NGC 1750 and NGC 1758

do not constitute a binary cluster (like h+χ Per), but an optical pair (like NGC 2451A and NGC 2451B; Platais et al. 1996).

More precise proper motions and photometry would allow to extend this analysis to fainter magnitudes. Additional data, such as metallicities and radial velocities, would improve the membership determinations.

Acknowledgements. The authors are very grateful to the referee, J.-C. Mermilliod, for his valuable comments, that greatly contributed to improve this paper. Many thanks also to B. Chen for his suggestions on preliminary versions of this paper.

This work has been supported by CYCIT under contracts ESP95-0180 and ESP97-1803, and by DGPC. D.G.-E. acknowledges partial support from the Spanish Ministerio de Educación y Ciencia (ref. AP92 30526274) and the Universitat de Barcelona.

References

Andersen J. 1991, A&AR 3, 91
Böhm-Vitense E., Canterna R. 1974, ApJ 194, 629
Cabrera-Caño J., Alfaro E.J. 1985, A&A 150, 298
Cabrera-Caño J., Alfaro E.J. 1990, A&A 235, 94
Cameron L.M. 1985, A&A 147, 47
Chen B., Asiain F., Figueras F., Torra J. 1997, A&A 318, 29
Chen B., Carraro G., Torra J., Jordi C. 1998, A&A, 331, 916
Cuffey J. 1937, Annals Harvard Obs. 105, 403
Dreyer J.L.E. 1888, New General Catalogue of Nebulae and Clusters of Stars, in Mem. Roy. Astron. Soc. 49
ESA 1997, The Hipparcos and Tycho Catalogues, ESA-SP 1200
Figueras F., Torra J., Jordi C. 1991, A&AS 87, 319
Flannery B.P., Johnson B.C. 1982, ApJ 263, 166
Francic S.P. 1989, AJ 98, 888
Galadí-Enríquez D., Jordi C., Trullols E., Ribas I. 1998a, A&A 333, 471 (Paper I)
Galadí-Enríquez D., Jordi C., Trullols E., et al. 1998b, A&AS, in press (Paper II)
Hand D.J. 1981, Discrimination and Classification, John Wiley & Sons ltd.
Hand D.J. 1982, Kernel Discriminant Analysis, Chichester Research Studies Press
Janes K.A., Tilley C., Lyngå G. 1988, AJ 95, 771
Jasniewicz G. 1984, A&A 141, 116
King I. 1962, AJ 67, 471
Kozhurina-Platais V., Girard T., Platais I., et al. 1995, AJ 109, 672
Lennon D.J., Dufton P.L., Fitzsimmons A., Gehren T., Nissen P.E. 1990, A&A 240, 349
Leonard P.J. 1988, AJ 95, 108
Lyngå G. 1982, A&A 109, 213
Marschall L.A., Van Altena W.F. 1987, AJ 94, 71
Masana, E. 1994, Degree of Physics, Universitat de Barcelona
McCarthy M.F, Treanor S.J. 1965, Ricerche Astronomiche 7, 177
McCuskey S.W. 1941, ApJ 94, 468
Mermilliod J.-C. 1981, A&A 97, 235
Meynet G., Mermilliod J.-C., Maeder A. 1993, A&AS 98, 477
Phelps R.L., Janes K.A. 1993, AJ 106, 1870
Platais I., Kozhurina-Platais V., Barnes S., Horch E.P. 1996, BAAS, 188, 3
Röser S., Bastian U. 1989, PPM-Positions and Proper Motions-North, Astron. Rechen. Inst.
Sagar R., Cannon R.D. 1997, A&AS 122, 9
Sanders W.L. 1971, A&A 15, 173
Schilbach E., Robichon N., Souchay J., Guibert J. 1995, A&A 299, 696
Schaller G., Schaerer D., Meinet G., Maeder A. 1992, A&AS 96, 269
Silverman B.W. 1986, Density Estimation for Statistics and Data Analysis, J.W. Arrowsmith Ltd.
Slovak M.H. 1977, AJ 82, 818
Soubiran C. 1992, PhD thesis, Observatoire de Paris
Stetson P.B. 1980, AJ 85, 387
Straižys V. 1992, Multicolor Stellar Photometry, Astronomy and Astrophysic Series Vol. 15, Pachart Publishing House
Straižys V., Černis K., Meištas E. 1992a, Baltic Astronomy 1, 125 (SČM)
Straižys V., Černis K., Kazlauskas A., Meištas E. 1992b, Baltic Astronomy 1, 149
Twarog B.A., Ashman K.M., Anthony-Twarog B.J. 1997, AJ 114, 2556
Vasilevskis S., Klemola A., Preston G. 1958, AJ 63, 1262
Vasilevskis S., Sanders W.L., Balz A.G.A. 1965, AJ 70, 797
Vázquez R.A., Baume G., Feinstein A., Prado P. 1997, A&AS 124, 13
Wilner D.J., Lada Ch.J. 1991, AJ 102, 1050
Worley C.E., Douglas G.G. 1984, The Washington Visual Double Star Catalog, US Naval Obs.
Zhao J.L., He Y.P. 1990, A&A 237, 54
Zhao J.L., Shao Z.Y. 1994, A&A 288, 89